Atomistic Investigation of Load Transfer Between DWNT Bundles "Crosslinked" by PMMA Oligomers

Mohammad Naraghi, Graham H. Bratzel, Tobin Filleter, Zhi An, Xiaoding Wei, SonBinh T. Nguyen, Markus J. Buehler, and Horacio D. Espinosa**

The production of carbon nanotube (CNT) yarns possessing high strength and toughness remains a major challenge due to the intrinsically weak interactions between "bare" CNTs. To this end, nanomechanical shear experiments between functionalized bundles of CNTs are combined with multiscale simulations to reveal the mechanistic and quantitative role of nanotube surface functionalization on CNT-CNT interactions. Notably, the in situ chemical vapor deposition (CVD) functionalization of CNT bundles by poly(methyl methacrylate) (PMMA)-like oligomers is found to enhance the shear strength of bundle junctions by about an order of magnitude compared with "bare" van der Waals interactions between pristine CNTs. Through multiscale simulations, the enhancement of the shear strength can be attributed to an interlocking mechanism of polymer chains in the bundles, dominated by van der Waals interactions, and stretching and alignment of chains during shearing. Unlike covalent bonds, such synergistic weak interactions can re-form upon failure, resulting in strong, yet robust fibers. This work establishes the significance of engineered weak interactions with appropriate structural distribution to design CNT yarns with high strength and toughness, similar to the design paradigm found in many biological materials.

1. Introduction

Since their reported discovery in 1991, carbon nanotubes (CNTs) have attracted considerable attention both in scientific research and industrial applications.[1–5] A promising aspect of research in this field, motivated by the extraordinary physical properties of CNTs, such as their high strength, good thermal stability, and excellent electrical properties, is the development of high-performance nanocomposites.[6–18] More recently, an active research direction related to CNT nanocomposites has been the fabrication of macroscopic nanotube yarns, with CNTs as their primary constituents, mainly for structural applications.[16,18–21] However, due to the weak interactions between CNTs, the remarkable properties of CNTs measured at the nanoscale have not yet been translated to the macroscale.[18,22] These limitations present a fundamental barrier that currently hinders the widespread application of CNT-based materials, including related carbon nanostructures such as graphene.

Studies at the atomistic and nanometer scales have proven to be instrumental in developing a fundamental understanding of interactions between CNTs. These studies have pointed to a wide range of interfacial shear strengths between graphitic surfaces from $\approx$0.08 MPa to several tens of MPa, depending on the surface chemistry of the CNTs and their surface defect density. One of the first studies in probing the interactions between CNT shells was a set of experiments reported by Cumings and Zettl, in which the inner shells of a multiwalled CNT were pulled out of the outer shell in a reversible and nearly friction-free process.[23] In our own previous work, we have applied an in situ transmission electron microscopy (TEM) method to measure the shear force needed to produce sliding between the inner and outer shells of multiwalled CNTs.[24] An average post-failure force of 35 nN was measured, required to pull out the 11 inner shells of a 14 nm diameter multiwalled CNT, with respect to the outer shell. Yu et al. measured the interfacial shear strength between shells of multiwalled CNTs (MWNTs) to be in the range of 0.08–0.3 MPa.[25] More-recent studies have demonstrated that the interfacial shear strength between pristine MWNTs is about 56 MPa.[26] However, with these levels of interfacial shear strengths, larger-scale CNT yarns typically fail due to weak junctions, at stresses well below the intrinsic strength of the CNTs.[22] As a result, the remarkable mechanical properties of CNTs are invisible at the macroscale.

To enhance further the shear interactions between CNTs, several approaches have been implemented, such as e-beam

Dr. M. Naraghi,[+] Dr. T. Filleter,[++] Dr. X. Wei,
Prof. H. D. Espinosa
Micro and Nanomechanics Laboratory
Department of Mechanical Engineering
Northwestern University
2145 Sheridan Road, Evanston, Illinois 60208-3111, USA
E-mail: espinosa@northwestern.edu

G. H. Bratzel, Prof. M. J. Buehler
Laboratory for Atomistic and Molecular Mechanics (LAMM)
Department of Civil and Environmental Engineering
Massachusetts Institute of Technology, 77, Massachusetts Ave.
Cambridge, MA, USA
E-mail: mbuehler@mit.edu

Z. An, Prof. S. T. Nguyen
Department of Chemistry
Northwestern University
2145 Sheridan Rd, Evanston, Illinois 60208-3113, USA

[+] Present address: Department of Aerospace Engineering, Texas A& M University, 3141 TAMU, College Station, TX 77843-3141, USA

[++] Present address: Department of Mechanical and Industrial Engineering, University of Toronto, 5 King's College Rd., Toronto, ON, M5S 3G8, Canada

DOI: 10.1002/adfm.201201358

irradiation crosslinking, and chemical or physical functionalization of CNTs.[2,24,27–31] In the former method, the shells of the CNTs are covalently crosslinked by e-beam irradiation, which transforms the sp^2-hybridized C atoms in each shell into pairs of sp^3-hybridized C–C linkages between shells. In the latter methods, the interactions between the CNTs are enhanced via intermediary polymer molecules and functional groups. By performing nanoscale pull-out experiments, Barber et al. demonstrated that physical and chemical interactions can increase the interfacial shear strength between CNTs and polyethylene (PE) to as high as 20–130 MPa.[32] On the other hand, Espinosa and co-workers showed that CNT-CNT junctions can reach an interfacial shear strength as high as 60 MPa if the junction overlap length exceeds a certain critical value.[26] Therefore, higher interfacial shear strength values can be mostly attributed to polymer chains wrapping around the CNTs, to van der Waals interactions (i.e., physical interactions), and to potential covalent bond formation between these chains and defect sites on the CNTs.[32,33] Cooper et al. measured the interfacial shear strength between single-walled CNTs and an epoxy resin to be as high as 366 MPa, potentially due to covalent crosslinks that could develop between the matrix and defect sites on CNTs.[34]

In addition to experimental synthesis efforts to create advanced CNT-based composites, bottom-up computational approaches have proven to be a powerful means for investigating atomistic-scale interactions in carbon-nanotube composite materials by revealing possible systems and configurations that warrant experimental and physical realization. Such approaches have included quantum-mechanics studies,[35,36] full atomistic molecular mechanics or molecular dynamics,[24,37] and coarse-grain models[38] that have investigated the interactions between carbon nanotubes and the various material interfaces. Molecular-dynamics simulations of the interactions between CNTs and polyethylene suggest that van der Waals interactions between CNT and polyethylene can result in an interfacial shear strength of ≈2.8 MPa, while even a low density of chemical crosslinks can substantially enhance the shear strength. In the case of crystalline polyethylene with ≈1% crosslinking density, the enhancement in the shear strength was estimated to be as high as 100 MPa.[37] Other simulation studies have suggested that the interfacial shear strength between CNTs and polyethylene chains can be substantially enhanced by the chemical functionalization of CNTs with radicals such as phenyl, which remain perpendicular anchored to the CNTs, thus delaying the slippage of the PE molecules across the surface of the CNTs.[39] Similarly, atomistic modeling has demonstrated that the physical interactions (both electrostatic and van der Waals) between CNTs and polymers such as polystyrene may result in interfacial shear strengths that are several times stronger than interactions between microfiber-reinforced composites.[40,41]

As discussed in the previous paragraphs, previous studies have mainly considered two approaches to enhance the interactions between CNTs in CNT yarns: covalently crosslinked CNT shells, obtained through e-beam irradiation of CNTs or bundles of CNTs,[2,31] and impregnation of CNT yarns with polymer matrices that interact favorably with the CNTs.[9,42] In the latter approach, chemical functionalization of the tube surfaces can yield functional groups that interact favorably with those of the polymer chains and substantially improve the load transfer between CNTs.[35,39,40] Both approaches exhibit a trade-off between strength, modulus, and toughness, as is common in most engineering materials. The former method, covalent bonding between CNT shells, will result in strong interlayer bonds (thus a gain in material stiffness and strength), at the expense of material toughness. The loss of material toughness is expected to be due to the directional preference of the covalent bonds and their relatively low interaction range, which make them vulnerable to local stress concentrations. In the second approach, polymer intermediary molecules can substantially increase the interactions between CNTs in CNT-based yarns by a host of mechanisms such as forming covalent bonds with CNTs, increasing the contact area of CNTs by wrapping around CNTs, etc.[39] However, because the strength of such a "polymer-crosslinked" CNT yarn will be limited by the strength of the polymer matrix, which is typically a very small fraction of the strength of CNTs, this approach will likely sacrifice strength for toughness.

Herein, we report a strategy that can reconcile high strength and high toughness in CNT yarns by enhancing the shear interactions between bundles of double-walled nanotubes (DWNTs) with a combination of weak (van der Waals) interactions and covalent bonds. Our approach is based on the incorporation of short polymer chains (oligomers) that are covalently bonded to the surfaces of DWNT bundles, as anchors to develop weak van der Waals interactions with neighboring CNTs. As shown by both nanomechanical experiments and multiscale simulations, such a synergistic combination of interactions does not sacrifice either strength or toughness of the bundle-bundle junction. Our material choice was driven by a recipe previously developed for floating-catalyst chemical vapor deposition (CVD) growth of CNTs possessing a very narrow distribution in the number of shells and diameters (more than 97% DWNTs),[18] which facilitates data analysis and sample geometrical characterization.

2. Results and Discussion

2.1. Polymer-Coated Double-Walled CNT Bundles and Yarns

The double-walled CNT bundles investigated in this manuscript were synthesized at the MER Corporation (details of their synthesis and structure are included in the Methods Section). We have previously demonstrated that this same DWNT bundle material can be spun into macroscopic fibers that exhibit high strength and toughness similar to that of natural spider silk.[18] In this previous study, the lateral interactions between adjacent "polymer-coated" bundles in the fibers were identified as an important component of their excellent mechanical properties; however, the mechanical behavior of bundle-bundle interactions and the mechanisms associated with these interactions remained unknown. The characterization of the native (i.e., intrinsically present on the surface of the bundles as a consequence of the DWNT synthesis) polymer coating of the bundles using X-ray photoelectron spectroscopy (XPS), Fourier transform infrared (FTIR) spectroscopy,[43] thermogravimetric analysis, and mass spectrometry (TGA-MS)[18] have previously been reported. This intrinsic polymer coating was found to

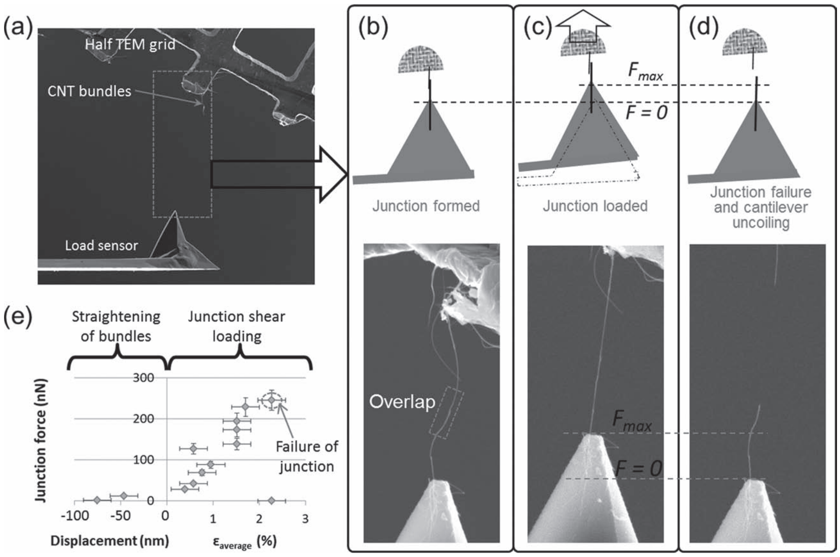

Figure 1. a) In situ SEM testing set-up used to investigate the shear interactions between DWNT bundles. b–d) A junction between the bundles is formed inside the SEM with a range of overlap lengths up to 1 μm (b), followed by loading the junction in shear mode (c), until junction failure occurs (d). The dashed lines indicate the location of the cantilever tip under maximum load and zero load configurations. e) Plot of junction force as a function of the stage motion and average axial strain in the bundles.

comprise mostly of acrylate moieties along with the presence of alkyl, carbonyl, carboxyl, hydroxyl, and ester functional groups, as detected by XPS and FTIR spectroscopy. Further analysis of the organic-soluble portion of this polymer coating by nuclear magnetic resonance (NMR) spectroscopy showed strong peaks with chemical shifts associated with esters (2.1–2.3 ppm and 4.2–4.5 ppm), hydroxyl groups (3.4–3.8 ppm), and alkyl-based substituents and the backbone (1–2 ppm), as well as small peaks with shifts associated with aromatic protons (7.6–8.4 ppm) and carboxyl groups (10.8 ppm) (see NMR spectra in the Supporting Information). Therefore, we hypothesize that this polymer coating is predominantly alkyl-substituted polyacrylates, with minor components being aromatic rings, carboxyl groups, and hydroxyl groups.

2.2. Nanomechanical Characterization of Bundle Junctions

The experimental nanomechanical characterization of the double-walled CNT bundle junctions was carried out using both in situ scanning electron microscopy (SEM) and TEM by loading a bundle pair junction in shear mode. In SEM, an atomic force microscopy (AFM) cantilever with known stiffness was used as the load sensor, as shown in **Figure 1**a. One double-walled CNT bundle was mounted on the AFM cantilever. Using a nanomanipulator inside an electron microscope, the bundle on the cantilever tip was brought near, and approximately parallel to, another cantilevered bundle protruding from a TEM grid. When the distance between the bundles was sufficiently small, the bundles slightly bent toward each other, likely due to electrostatic interactions within the SEM chamber, and formed a junction. More details of sample manipulation procedures are presented in the Methods Section. Figure 1b–d shows subsequent SEM images of a shear experiment including the formation of a bundle-bundle junction (Figure 1b), pulling the two bundles apart from each other and loading the junction (Figure 1c) until junction failure (Figure 1d). Using the above protocol, each DWNT bundle will be loaded in tension, while their junction will dominantly experience a shear stress parallel to the interface.

The force on the bundles as a function of overall average axial strain is shown in Figure 1e, where the average strain was calculated as the total axial deformation of the bundle pair with respect to its initial length. The initial slack of the sample was excluded from the total deformation to calculate the average axial strain. For the experimental data plotted in Figure 1e, the failure force was measured to be ≈250 nN. In all of the SEM experiments, the overlap length between the two bundles was systematically varied but kept below 1 μm, since at higher overlap lengths, bundle failure rather than failure of the junctions was observed. Because the experiment was performed under load control, in all cases the junction failure was abrupt, and no sliding was detected prior to failure.

2.3. Multiscale Modeling

To extract the details of the molecular interactions and deformation mechanisms during bundle shearing, we utilized an atomistically trained coarse-grain simulation approach that allowed for the investigation of the structural and mechanical properties of the polymer-coated CNT bundles. While molecular-level interactions of adjacent carbon nanotubes has been extensively investigated using atomistic methods,[44–48] bundles and fibers consisting of a large number of CNTs, as studied here, become too computationally expensive at the atomistic level (see Supporting Information, Figure S2). Moreover, simulating polymer crosslinks further adds to the computational cost. Hence, mesoscopic "bead-spring" methods were employed as a viable approach to simulate arrays of CNTs[49–51] that can reach the same scales as those investigated in our experimental studies.

A "fine-trains-coarse" multiscale approach was implemented to produce a mesoscale model derived from atomistic calculations[49,50] (further details of the simulation of the bundles and their junction, as well as validation of the coarse-grain model, are presented in the Methods Section and in the Supporting Information). The dimensions of the modeled bundles and the density of polymer chains on the surface were identified experimentally (see Methods Section and the Supporting Information). The polymer chains on bundles were modeled as poly(methyl methacrylate) (PMMA) (a prototypical alkyl-substituted polyacrylate) oligomers with lengths of 4 or 8 repeating units based on their similarities to the chemical structure of the inherent polymer coating obtained through XPS, FTIR and NMR spectroscopy, and TGA-MS analysis.[18,43] The choice of

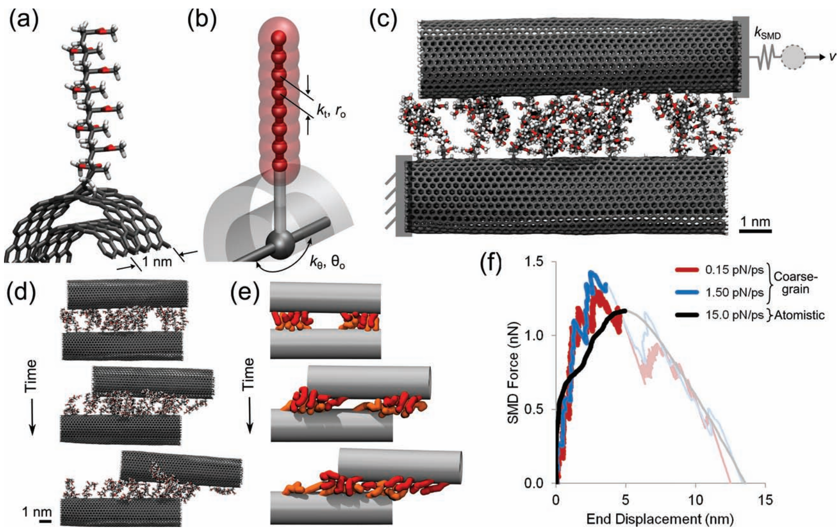

Figure 2. Validation of the coarse-grain model by comparison with atomistic shear behavior at the same length scale. a) Components of the bundle: ultrashort PMMA oligomer covalently bonded to the sidewall of a DWNT. b) Coarse-grain (bead-spring) representation of atomistic components, with effective physical dimensions derived from intermolecular adhesion parameters (Non-dimensional beads and springs are shown as opaque, while physical dimensions are shown as translucent). c) Setup of the SMD, showing virtual springs and dummy atoms. d,e) Snapshots of the atomistic (d) and coarse-grain (e) shearing of the "oligomer-crosslinked" interface during the molecular simulation. f) Force–displacement profiles show loading (solid line) and free acceleration after slipping (faded line), indicating good agreement between the atomistic and coarse-grain models.

polymer length in simulations was guided by gel-permeation chromatography (GPC) analysis that showed this polymer to have a molecular weight of 520 g mol^{-1} and a polydispersity index (PDI) of 1.1. This is consistent with a PMMA chain with an average degree of polymerization of 5, which is within the range used for the simulations.

To validate the development of the coarse-grain model, its response under simple shear of the "polymer-crosslinked" interface was compared with the response of an atomistic model of the same system. This system represents a small segment of the shear surface of the bundle-bundle junctions and represents an upper bound of the system size for atomistic simulations using a reactive potential with the available computational resources. The atomistic model consisted of two parallel DWNTs 10 nm in length with syndiotactic 8-mer PMMA chains covalently attached along the DWNT sidewall (**Figure 2**a). The equivalent coarse-grain (bead-spring) components are shown in Figure 2b, indicating with physically relevant dimensions derived from the intermolecular adhesion parameters. Non-dimensional beads and springs are shown as opaque in Figure 2b, while the physical dimensions are shown as translucent Each bead of the tubes on the bundle surface was bonded to a coarse-grain model of a PMMA oligomer.

Simple shear of the "oligomer-crosslinked" interface was accomplished via steered molecular dynamics (SMD), whereby the atoms of one tube, at $x = 0$, are held fixed in space, and the center of mass of the group of atoms of the second tube, at $x = L$, is connected by a harmonic spring potential to a massless "dummy atom" that moves at a constant velocity in the longitudinal direction (Figure 2c). Thus the force on the pulled group of atoms increases monotonically until the oligomer interface fails, and the top tube freely accelerates towards the dummy atom. During the shearing simulations of the atomistic (Figure 2d) and coarse-grain (Figure 2e) models, it was observed that the "crosslinks" aggregate via weak interactions, then become elongated and more aligned in parallel as the pulled DWNT displaces. Plotting the force in the SMD spring potential against the end displacement of the pulled tube allows direct comparison of the "crosslinked" interface shear behavior between the atomistic and coarse-grain models (Figure 2f). While the atomistic model must be loaded at 15.0 pN ps^{-1}, to perform the simulations within a convenient user timeframe (as dictated by current computational resources), the force–displacement profile shows good agreement with coarse-grain models of multiple orders of magnitude of loading rate.

The junctions tested experimentally (**Figure 3**a,b), were modeled using an assembly of two DWNT bundles with increasing overlap lengths of 100, 500, and 1000 nm) (Figure 3c,d). After equilibration, the junctions were loaded in shear. Figure 3e depicts the shearing force as a function of relative displacement of two bundles with an overlap length of 100 nm. At a deformation below ≈7 nm, the relative sliding between the tubes is mostly accommodated by the shear deformation of the polymer coating (cf. Figure 3f,g). This simulation prediction is consistent with our TEM bundle-shear measurements as explained in the next section. Given an average spacing between bundles of ≈2.5 nm, this amount of shear deformation corresponds to shear strains of ≈300%. This massive shear strain on the oligomers stretches them, resulting in more contact area between the chains and the two bundles and thus enhanced shear interactions. In the simulations, the junction failure forces correspond to the bundles overcoming the crosslinking adhesion at the interface, as manifested by the beginning of slip without sticking (Figure 3e). Further loading of the junction results in a sudden increase in the junction displacement, in agreement with our experimental observations of abrupt junction failure.

2.4. In situ TEM and SEM Studies of Junction Failure and Associated Multiscale Simulations

Because in situ SEM lacks the resolution needed to capture the predicted sliding (below ≈7 nm) between the two bundles prior to junction failure, we also undertook in situ TEM studies. For this purpose, a pair of bundles with an overlap length of ≈1.4 μm were mounted on the gripping pads of a micro-electromechanical system (MEMS)-based tensile stage,[2,31,52] as shown in Figure 3a,b. Upon actuating the device, the gripping pads were moved apart from each other, loading the junction in shear. Using image correlation to track the relative motion

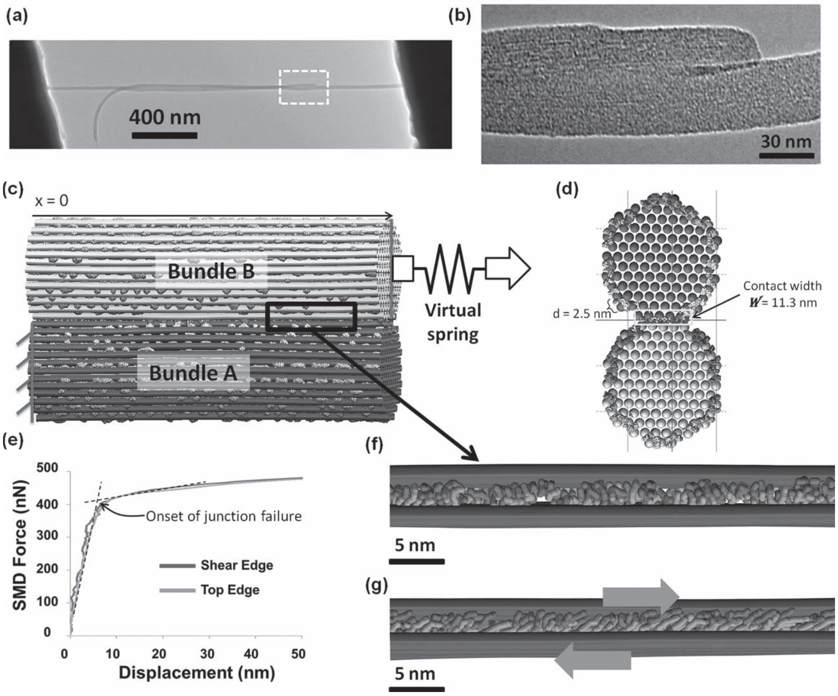

Figure 3. a) TEM image of two overlapping DWNT bundles mounted on a MEMS testing stage. b) High-resolution TEM image of the end of one of the DWNT bundles (from the region indicated in (a)). c,d) Side view (c) and cross-section (d) of the coarse-grain model of a bundle pair used in the multiscale simulations. The diameter of each bundle is ≈26 nm. e) The SMD sliding force as a function of the relative displacement between the two bundles. f,g) The oligomers at the shear surface are well-mixed at zero load (f) and elongate and align when the bundle pair is sheared (g).

between the two ends of the bundle junction, the sliding between the two bundles was measured to be ≈10 nm, consistent with the simulation predictions on shorter junctions (Figure 3e). We note that while the TEM experimental set-up allowed for a much higher image resolution, the in situ SEM set-up was found to be more suitable for investigations of the shear interactions between bundles as a function of overlap length. Indeed, mounting DWNT bundles on the MEMS platform with controlled overlap lengths proved to be difficult and of low yield.

A complete set of in situ SEM-based experimental measurements and associated multiscale simulation results is presented in **Figure 4**. In this Figure, the critical junction force (i.e., slip force) is normalized by the contact width to allow for a direct comparison of experimental and simulation results obtained from shearing bundles with different diameters. Following the multiscale simulation results of the bundle interactions, Figure 3d, the contact width between the bundles was taken as ≈0.40 of the average of the bundle pair diameter. The contact width was also used to estimate the average shear strength, as the ratio of the critical junction force to contact area. Each data point in Figure 4 corresponds to the junction failure force for a particular experiment. As shown in this Figure, the junction slip force does not scale linearly with overlap. At small overlap length, below ≈250 nm, the junction failure force per unit width vs. overlap length can be approximated by a straight line (using the least-squares method), with a slope of ≈330 ± 80 MPa, regarded as the average interface shear strength of the junction. Note that the failure force for a given overlap length is expected to have a statistical variation and this is exactly what the experimental data shows. Part of this variation can also be attributed to experimental errors, as discussed in the experimental section.

Multiscale simulations further reveal the dependence of the slip force per unit width on the overlap length as shown in Figure 4. At the smallest overlap length studied in the simulations (100 nm), the average interface shear strength is ≈394 MPa, which drops by 23% and 43% as the overlap length is increased to 500 nm and 1 μm, respectively. As stated earlier, this loss in the average interfacial shear strength is attributed to non-uniform distribution of the shear stress along the interface.[26] The magnitude of this non-uniformity, predicted by the shear-lag model (see discussion below), is reduced at shorter overlap lengths. Thus, the higher limit (≈394 MPa),

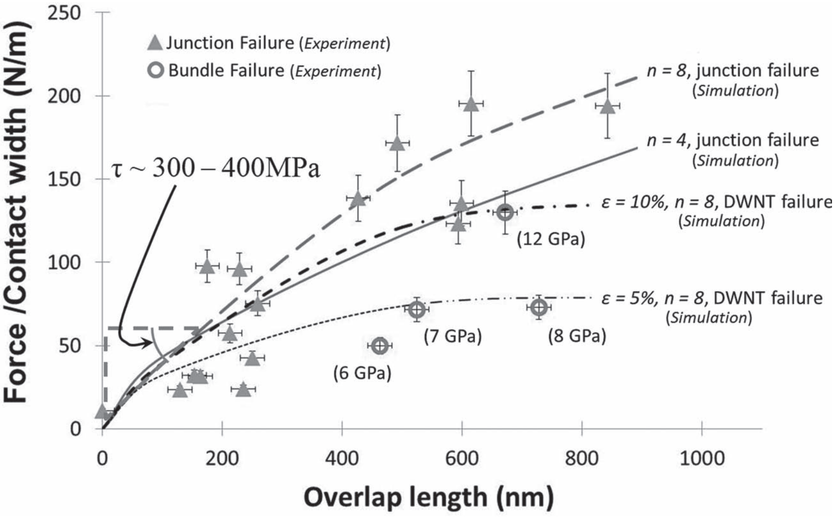

Figure 4. Plots of junction critical force vs. overlap length obtained by nanomechanical shear in situ SEM experimental and multiscale simulations. The experimental data is shown as individual points and the simulation results are plotted as curves. The solid data points correspond to bundle junction failure, while the open circles represent bundle failures (in the latter case, the strength of the bundles is shown in brackets). The solid and dashed lines represent the simulation results with 4- and 8-mer chains, in which the junction has failed. The two broken-line curves represent the DWNT failures obtained in simulations for the 8-mer case at 5 and 10% strains.

which is obtained at the smallest overlap length, is a better approximation of the true value of the junction shear strength. A similar trend is observed for shorter PMMA oligomers (four repeating units), with a shear strength of ≈400 MPa at small overlap lengths, which drops by as much as 58% as the overlap length reaches 1 μm, indicating a considerable dependence of the average shear strength on overlap length.

The dependency of the junction slip force as a function of overlap length can be explained by a shear-lag model,[26] which predicts that the shear stress is the highest at the ends of the overlap length (where failure initiates at a critical shear stress value) and drops towards the center of the junction.[26] For longer overlap lengths, the shear stress is very small in the center of the junction over a large fraction of the total overlap. Thus, for a given critical shear stress, the average shear stress will decrease with overlap length, resulting in a reduction of the critical force per unit overlap length. This trend also suggests that at a sufficiently long overlap length, the critical junction force reaches saturation.[26] In the experiments reported here, when the overlap length was in the range of ≈850 nm to ≈1 μm, a transition in failure mode occurred with failure shifting to bundle failure rather than interface failure. Because of this, the full saturation of the failure force could not be measured experimentally. Interestingly, this finding shows that the polymer coating present in the tested MER DWNT bundle material has the potential to maximize the load transfer in a yarn made of discontinuous double-walled CNT bundles and, consequently, maximize the load carrying capacity of the yarn. Moreover, it reveals that the full potential of the double-walled CNT bundles was not achieved in the yarns previously studied by us,[18] primarily due to lack of alignment and crosslinking within the bundles.[31] We note that the value of interfacial shear strength between the bundles (300–400 MPa), consistently measured in our experiments and predicted by our multiscale simulations, are among the highest values measured in CNT-based composite structures, pointing to the remarkable effectiveness of the in situ CVD functionalization (i.e., the intrinsic polymer coating) in enhancing the interactions between CNTs.[25,32,33]

2.5. Mechanism of Enhanced Strengthening of the Interface Between the Polymer-Coated CNT Bundles

Further insight into the mechanisms that operate during the deformation of junctions leading to high interfacial shear strength is obtained through the coarse-grain molecular-dynamics simulations. The interactions between the two bundles are dominated by van der Waals interactions between the oligomers on their surfaces. The lack of directional preference and relatively long interaction ranges of van der Waals forces facilitates the formation of non-covalent bonds between two bundles, when they are sufficiently close to each other. Due to their backbone flexibility, the oligomers on the surfaces of one bundle can conform to the shape of the other bundle, leading to more van der Waals interactions (see Supporting Information for conformation of both coarse-grained and atomistic oligomers). The chain flexibility, which scales with oligomer length, is a consequence of the rotational degree of freedom of the carbon-carbon covalent bonds about their bond axis in PMMA oligomers. This explains why bundles with longer oligomers can form stronger shear interfaces. While the 4- and 8-mer PMMA chains are represented in the coarse-grain model at the same density, the 8-mer is able to reach twice as far from the nanotube sidewall to find neighbors for non-covalent interaction. The shorter 4-mers require much better alignment and closer proximity of the bundle pair before loading, and they cannot restructure as much as the 8-mers, directly preceding slipping at the interface. Therefore, the longer 8-mers create a stronger and more-robust "crosslinked" interface, and it is quite likely that still-longer oligomers would increase levels of interaction and entanglement, and thus the overall strength of the interface.

A key mechanism in the strengthening of the interface between the bundles during loading is the extension and alignment of the oligomers at the shear surface. Similar to junction formation, this mechanism is also a consequence of oligomers flexibility (due to the rotational degree of freedom of C–C bonds in PMMA oligomers, as explained earlier), lack of directional preference of van der Waals interactions, and the capability of individual non-covalent bonds to re-form subsequent to their failure. The latter is of particular importance to develop nanoscale interfaces with high toughness. After equilibration of the initial bundle-pair structure, the coarse-grain oligomers at the shear surface are observed to be well-mixed, clumped into groups, and kinked. When force is applied to the end of the loaded bundle, the bundles initially slip while the oligomers are extended and become aligned, as shown in Figure 3f,g. This alignment allows for the close interaction of many more oligomer side-groups and an enhancement of the interface. A similar behavior was also observed in the atomistic simulation used to validate the coarse-grain models (see Supporting Information). Altogether, the shear strength between the bundles is enhanced by interplay between the strong covalent bonds, within each of the PMMA oligomers, and the weak van der Waals interactions between the oligomers on the surfaces of the two bundles. It is interesting to note that the overall adhesion of these weak, non-covalent interactions is sufficient to resist shearing between the bundles until hundreds of MPa of shear stress is applied along the interface.

2.6. Experimental Uncertainty and Possibility of Bundle Failure

The shear strength values calculated so far from simulations correspond to the case when five double-walled CNTs on each bundle are along the interface, as shown in Figure 3d. However, depending on the initial orientation of the bundles with respect to each other (see TEM images in Figure 3a,b), less energetically favorable junctions can also form between bundles in which a lower number of double-walled CNTs (three to four) from each bundle lie along the bundle-pair interface, as shown in **Figure 5**a,b. The coarse-grain model also allows for the investigation of the effect of contact width for a given bundle diameter on the shear interactions between bundles. In such cases, and for the 8-mer long PMMA chains and an overlap length of 100 nm, the multiscale simulations predict that the critical junction force is reduced by ≈20%, which corresponds to a loss of the interface shear strength of ≈8%, as shown in Figure 5c. Therefore,

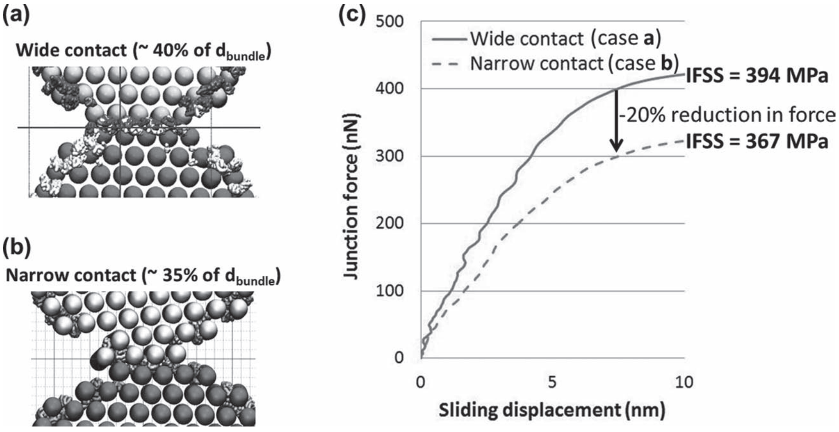

Figure 5. Due to the uneven surfaces of the bundles, the number of DWNTs along the interface of the bundles depends on the initial orientation of the bundles with respect to each other. a,b) Two cases with 5 (a) and 3–4 (b) DWNTs along the interface. c) The higher number of DWNTs along the interface promotes interactions between the bundles, enhancing the slip force of the junction.

the experimental uncertainty in the number of double-walled CNTs along the interface in the shear experiments, which stems from the SEM resolution, may lead to a scatter range of ≈20% in the experimentally measured slip forces.

The experimental and simulation results presented thus far have focused on the failure of the interface between bundle pairs. However, in a more-generalized case, the junction between the bundles can be strong enough to prevent failure until the applied load is sufficient to break the bundles themselves. The probability of the latter scenario scales with the ratio of the junction slip force to bundle-pair failure force. Therefore, longer overlap lengths and the presence of defects in a bundle can result in bundle failure instead of interface failure. Experimentally, the failure of bundles instead of their junctions was observed in some instances at overlap lengths of 450 nm and above, as shown by the open circles in Figure 4. The true strength of the bundles in these cases is in the range of 6–12 GPa, with the corresponding strain to failure (estimated as the strength divided by modulus, with the latter measured previously[18]) in the range of 3–6%. These mechanical properties are in the range of strains and strengths previously measured for the same materials, which are lower than the strength of defect-free CNTs, pointing to the not-insignificant effect of defects in promoting the failure of bundles.[2,18] A similar effect, bundle failure rather than junction failure, is observed in the multiscale simulations when defects are introduced into the tubes. By tracking the force at which any nanotube reaches a failure strain in the 4–10% range (bundle-failure strain), the coarse-grain simulations predict a reduced force per unit width vs. overlap-length failure envelope, as shown in Figure 4. For the 100 nm overlap-length case and in the presence of either 4- or 8-mer PMMA chains, a failure strain of 5% is sufficient for the junction interface to fail before nanotube failure. However, at overlaps of 0.5 and 1 μm, even a 10% failure strain is not sufficient to prevent nanotube failure before junction failure. This drastically decreases the effective shear strength of the CNT-CNT junctions and points to a saturation of the slipping force, beyond a critical overlap length of approximately 0.5 μm, as a result of bundle failure. For the case of the 8-mer PMMA chains, this saturation is particularly evident, as any nanotube failure strain in the 5–10% range results in approximately the same slipping force for either a 0.6 μm or 1 μm overlap length. Since the 4-mer oligomer interface is weaker, saturation is less drastic, but it is still observed.

3. Conclusion

In summary, we have carried out a combined experimental and multiscale simulation study to investigate the effect that intrinsic acrylate oligomer coatings have on the mechanical interactions between double-walled CNT bundles. The experiments have elucidated the role of overlap length, quantified the interface failure force, and served as benchmarks to verify the simulations, while the coarse-grain simulations have provided detailed description of interactions between the bundles beyond the spatial resolution of the experiments. Both the experimental and the simulation studies point to a substantial enhancement of the interfacial shear strength between bundles to as high as 400 MPa, which is among the highest values reported in the literature, and an order of magnitude higher than the shear strengths that can be reached by pure van der Waals interactions between pristine CNTs.[26] The strong interactions between the bundles were mostly due to non-covalent interactions between the intrinsic acrylate oligomer chains present on the surface of the bundles, which were greatly enhanced by the "interdiffusion" of these chains during the formation of the junction. Not surprisingly, longer polymer chains were capable of extending the interaction zone, thus creating a more-robust and stronger interface between the bundles. During loading, the elongation of these oligomers and their alignment significantly increased the effective contact area between the bundles, leading to enhanced effective interfacial shear strength. Together, these observations comprise a novel mechanism for enhancing the mechanical properties of CNT-based materials without the need for strong bonding: only weak interactions and an appropriate structural distribution of the building blocks are needed. While we have utilized DWNT bundles as a platform in this study, our results should be applicable to many similar materials, including single- and multi-walled carbon nanotubes, their corresponding bundles, as well as any other nanoscopic fibrous materials.

4. Methods Section

Fabrication and Characterization of Carbon Nanotubes: DWNT bundles were fabricated by the MER Corporation in a CVD reactor with C_2H_4 and CO as the precursors. Each bundle, with an outer diameter of ≈10–30 nm, was composed of dozens of DWNTs with an outer diameter of ≈2.2 nm (determined by the radial breathing modes in Raman spectroscopy) in a hexagonally closed packed structure. As fabricated, these bundles were functionalized (in situ CVD) with an intrinsic organic material dominated by chains of alkyl-substituted polyacrylates. The polymer content of the bundles was ≈22 wt%, as determined by thermogravimetric analysis.[18] Moreover, solvent extraction of the bundles only marginally reduced their polymer content, pointing to strong bonds between the polymer coating and the bundles, such as covalent bonds or π-stacking between the aromatic groups of the polymer coating and DWNT bundles. Despite the high polymer content of the DWNT bundles, the Raman spectrum points to a very low defect density of the bundles (D/G peak of ≈2%[18,43]). For the NMR spectroscopy analysis, non-covalently bound polymer was extracted from the DWNT bundles by sonicating an area (≈10 cm^2) of the mat in analytical-grade methyl ethyl ketone for 3 h. The solvent was removed under vacuum and the remaining white residue was dissolved in $(CD_3)_2CO$ and analyzed using an AVANCE III 500 MHz NMR spectrometer (Bruker Biospin, Billerica, MA). For the GPC analysis, the polymer coating was extracted by sonicating a larger sample of DWNT mat (≈200 cm^2) in analytical-grade methyl ethyl ketone for 8 h. The solvent was removed under vacuum and the remaining residue was dissolved in chloroform and analyzed by gel-permeation chromatography (GPC) against polystyrene standards (see Supporting Information, S3).

DWNT Bundle Manipulation and Shear Experiments: Individual DWNT bundles were isolated from the as-fabricated mats and deposited on Cu TEM grids by gently rubbing the grids over the mats. The outcome of this method of isolation was DWNT bundles, some of which were cantilevered from the grid, with overhanging lengths as long as a few micrometers, which was ideal for sample manipulation. The TEM grid was mounted on the SEM stage. Subsequently, by using a nanomanipulator in situ to an SEM, the AFM cantilever tip was brought in contact with the free-standing end of a bundle. Along the contact length, the bundle was welded to the cantilever tip via e-beam-induced carbon deposition. Care was taken to avoid unwanted carbon deposition and e-beam exposure along the rest of the sample. The cantilever-welded bundle was then cut from the TEM grid through e-beam-induced etching and brought in contact with another free-standing bundle to form a junction with a desired length. Subsequently, the two bundles were pulled apart, and the junction was loaded in shear until failure. During the course of the experiment, the support of the bundle, attached to the TEM grid, was displaced both away from (pulled axially) and perpendicular to the cantilever, to compensate for the lateral motion of the cantilever tip. The failure of the junction occurred abruptly. As such, the time evolution of failure was not captured. Given the fact that samples can have an out of plane (z) component, the cantilever was moved in the z direction to bring both bundles in focus, therefore minimizing the out-of-plane component. The displacement error bars were estimated to be equal to one pixel size of the SEM images in each direction. Similarly, the strain error bars were calculated as the ratio of the displacement errors to the taut length of the DWNT bundles. The uncertainty in the force, calculated as the product of the uncertainty in the cantilever stiffness and the cantilever deflection, was primarily a result of the uncertainty in the stiffness of the cantilever, as shown by Cooper et al.[53]

Multiscale Simulations: A series of full atomistic calculations of mechanical test cases (test suite) was implemented via classical molecular dynamics (MD) to derive a simplified set of parameters for describing the nanotube behavior at the mesoscale in a coarse-grain model.[51,54] The MD simulations were performed using the massively parallelized modeling code, LAMMPS,[55] capable of running in parallel on large computing clusters. To model a realistic polymer-coated DWNT bundle, a simulated assembly procedure was inspired by the experimentally observed self-assembly of the junction. A coarse-grain bundle of 113 hexagonally packed tubes was created with polymer "crosslinks" oriented perpendicular to the bundle surface. The effective diameter of each tube was taken as ≈2.2 nm, and the outer diameter of the bundle as ≈26 nm, both very close to the experimentally measured diameters of the tubes and the bundles, respectively. The polymer-coated DWNTs at the bundle surfaces were nonpristine, and therefore the elastic regime of their Young's modulus was conservatively estimated to be only 500 MPa. Each bead of the tubes on the bundle surface was bonded to one end of a coarse-grain model of a PMMA oligomer. Moreover, the mass, spring rate, and adhesion strength of each coarse-grained PMMA oligomer was scaled to correspond to 22 wt% polymer density, thereby representing approximately 5.6 atomistic oligomers. The latter was motivated by the density of the intrinsic polymer coating estimated based on thermogravimetric analysis of the mats of DWNT bundles in Ar.[18] Figure 3c depicts the coarse-grain bead-spring model of a coated nanotube. Parameters of the coarse-grain model, defined from atomistic results, are given in Table S1 in the Supporting Information.

The equilibrated bundle was duplicated and mirrored, and the two bundles were brought together over 0.5 ns at 300 K until van der Waals interactions brought the nanotubes and "crosslinks" within a final equilibrium distance. This assembly process was repeated for each combination of tube length (100, 500, and 1 µm) and oligomer length (4- and 8-mer). The length of the oligomers was guided by experimental gel-permeation chromatography (GPC) analysis of the polymer coating on the DWNT bundles. Moreover, the simulated range of oligomer lengths represents the upper and lower bounds on the oligomer lengths observed in the experiments, thus providing an envelope for the predicted shear strengths.

It is to be emphasized here that accurate knowledge about the length of the chains and its distribution in the tested samples, is not a trivial task and has not been carried out here. Therefore, a comparison between $n = 4$ and $n = 8$ (4- and 8-mer, respectively) for junction failure, and the choice of $n = 8$ for CNT failure at $\varepsilon = 10\%$ and $\varepsilon = 5\%$ was made only to demonstrate the variations in junction critical force with either strain or polymer chain length. The case where both strain and chain length change, although of relevance in specific data analysis, was not pursued in this work where the emphasis is on explaining the two mechanisms leading to failure, as captured by the experimental results.

Mechanical Analysis in the Simulation: Shearing of the bundle-overlap interface was performed using steered molecular dynamics (SMD). Since each bundle pair represented the overlap site of much longer bundles, the beads at each end of the two bundles were constrained as a ridged body to approximate these boundary conditions. As shown in Figure 3c, the end of bundle A at $x = 0$ was fixed in space, while the end of bundle B at $x = L$ was loaded by a virtual spring with a spring rate and dummy atom velocity corresponding to a loading rate of 150 pN ps^{-1}. To determine a reasonable and convenient loading rate, preliminary tests were performed for short overlaps at both 10-times-slower and 10-times-faster load rates. The loading rate of 150 pN ps^{-1} was chosen for all shearing tests to optimize the computational efficiency without sacrificing data fidelity. At faster loading rates, the increase in force was so fast that the pulled end of the bundles slipped before crosslinking between the two bundles could take place, resulting in an unrealistic failure of the junctions. The latter is expected to be a limitation of the coarse-grain models and not of the impulse/impact reactions of the bundles.

Supporting Information

Supporting Information is available from the Wiley Online Library or from the author.

Acknowledgements

M.N. and G.H.B. contributed equally to this work. The authors gratefully acknowledge the support from ARO through a MURI award, No. W911NF-09–1-0541. We thank the MER Corporation and Dr. Alexander Moravsky for the synthesis of the DWNT bundles used in this work and insights regarding the composition of the intrinsic polymer coatings on the DWNT bundles. We are also grateful to Prof. George Schatz for his many insightful discussions on the chemistry of this intrinsic polymer coating. We acknowledge support from Dr. S. Li in the Electron Probe Instrumentation Center (EPIC) at Northwestern University for TEM imaging. All of the authors contributed to the design and analysis of the experiments and simulations, discussed the results, and wrote the paper. M.N., T.F., Z.A. and X.W. performed the experiments, and G.H.B. performed the simulations.

Received: May 18, 2012
Revised: August 3, 2012

---

[1] M. F. Yu, O. Lourie, M. J. Dyer, K. Moloni, T. F. Kelly, R. S. Ruoff, *Science* **2000**, *287*, 637.
[2] B. Peng, M. Locascio, P. Zapol, S. Li, S. L. Mielke, G. C. Schatz, H. D. Espinosa, *Nat. Nanotechnol.* **2008**, *3*, 626
[3] A. M. F. Lima, A. W. Musumeci, H. W. Liu, E. R. Waclawik, G. G. Silva, *J. Therm. Anal. Calorim.* **2009**, *97*, 257.
[4] L. S. K. Pang, J. D. Saxby, S. P. Chatfield, *J. Phys. Chem.* **1993**, *97*, 6941.
[5] E. Pop, D. A. Mann, K. E. Goodson, H. J. Dai, *J. Appl. Phys.* **2007**, *101*, 093710.
[6] Z. Spitalsky, D. Tasis, K. Papagelis, C. Galiotis, *Prog. Polym. Sci.* **2010**, *35*, 357.
[7] P. Miaudet, S. Badaire, M. Maugey, A. Derre, V. Pichot, P. Launois, P. Poulin, C. Zakri, *Nano Lett.* **2005**, *5*, 2212.
[8] G. L. Hwang, Y. T. Shieh, K. C. Hwang, *Adv. Funct. Mater.* **2004**, *14*, 487.
[9] M. S. P. Shaffer, A. H. Windle, *Adv. Mater.* **1999**, *11*, 937.
[10] M. Cadek, J. N. Coleman, V. Barron, K. Hedicke, W. J. Blau, *Appl. Phys. Lett.* **2002**, *81*, 5123.
[11] X. F. Zhang, T. Liu, T. V. Sreekumar, S. Kumar, V. C. Moore, R. H. Hauge, R. E. Smalley, *Nano Lett.* **2003**, *3*, 1285.
[12] W. J. Ma, L. Song, R. Yang, T. H. Zhang, Y. C. Zhao, L. F. Sun, Y. Ren, D. F. Liu, L. F. Liu, J. Shen, Z. X. Zhang, Y. J. Xiang, W. Y. Zhou, S. S. Xie, *Nano Lett.* **2007**, *7*, 2307.
[13] A. B. Dalton, S. Collins, E. Munoz, J. M. Razal, V. H. Ebron, J. P. Ferraris, J. N. Coleman, B. G. Kim, R. H. Baughman, *Nature* **2003**, *423*, 703.
[14] M. Zhang, S. L. Fang, A. A. Zakhidov, S. B. Lee, A. E. Aliev, C. D. Williams, K. R. Atkinson, R. H. Baughman, *Science* **2005**, *309*, 1215.
[15] K. Koziol, J. Vilatela, A. Moisala, M. Motta, P. Cunniff, M. Sennett, A. Windle, *Science* **2007**, *318*, 1892.
[16] Y.-L. Li, I. Kinloch, A. Windle, *Science* **2004**, *304*, 276.
[17] M. Motta, A. Moisala, I. A. Kinloch, A. H. Windle, *Adv. Mater.* **2007**, *19*, 3721.
[18] M. Naraghi, T. Filleter, A. Moravsky, M. Locascio, R. O. Loutfy, H. D. Espinosa, *ACS Nano* **2010**, *4*, 6463.
[19] M. D. Lima, S. L. Fang, X. Lepro, C. Lewis, R. Ovalle-Robles, J. Carretero-Gonzalez, E. Castillo-Martinez, M. E. Kozlov, J. Y. Oh, N. Rawat, C. S. Haines, M. H. Haque, V. Aare, S. Stoughton, A. A. Zakhidov, R. H. Baughman, *Science* **2011**, *331*.
[20] M. Zhang, K. R. Atkinson, R. H. Baughman, *Science* **2004**, *306*, 1358.
[21] B. Vigolo, A. Penicaud, C. Coulon, C. Sauder, R. Pailler, C. Journet, P. Bernier, P. Poulin, *Science* **2000**, *290*, 1331.
[22] J. J. Vilatela, J. A. Elliott, A. H. Windle, *ACS Nano* **2011**, *5*, 1921.
[23] J. Cumings, A. Zettl, *Science* **2000**, *289*, 602.
[24] M. Locascio, B. Peng, P. Zapol, Y. Zhu, S. Li, T. Belytschko, H. D. Espinosa, *Exp. Mech.* **2009**, *49*, 169.
[25] M. F. Yu, B. I. Yakobson, R. S. Ruoff, *J. Phys. Chem. B* **2000**, *104*, 8764.
[26] X. Wei, M. Naraghi, H. D. Espinosa, *ACS Nano* **2011**, *6*, 2333.
[27] N. G. Sahoo, H. K. F. Cheng, J. W. Cai, L. Li, S. H. Chan, J. H. Zhao, S. Z. Yu, *Mater. Chem. Phys.* **2009**, *117*, 313.
[28] X. D. Cao, H. Dong, C. M. Li, L. A. Lucia, *J. Appl. Polym. Sci.* **2009**, *113*, 466.
[29] W. Wang, P. Ciselli, E. Kuznetsov, T. Peijs, A. H. Barber, *Philos. Trans. R. Soc. A* **2008**, *366*, 1613.
[30] A. Kis, G. Csanyi, J. P. Salvetat, T. N. Lee, E. Couteau, A. J. Kulik, W. Benoit, J. Brugger, L. Forro, *Nat. Mater.* **2004**, *3*, 153.
[31] T. Filleter, R. Bernal, S. Li, H. D. Espinosa, *Adv. Mater.* **2011**, *23*, 2855.
[32] A. Barber, S. Cohen, H. D. Wagner, *Appl. Phys. Lett.* **2003**, *82*, 4140.
[33] A. H. Barber, S. R. Cohen, S. Kenig, H. D. Wagner, *Compos. Sci. Technol.* **2004**, *64*, 2283.
[34] C. Cooper, S. Cohen, A. Barber, D. Wagner, *Appl. Phys. Lett.* **2002**, *81*, 3873.
[35] K. Mylvaganam, L. C. Zhang, *J. Phys. Chem. B* **2004**, *108*, 5217.
[36] Y.-C. Liu, J.-W. Shen, K. E. Gubbins, J. D. Moore, T. Wu, Q. Wang, *Phys. Rev. B: Condens. Matter* **2008**, *77*, 125438.
[37] S. J. V. Frankland, A. Caglar, D. W. Brenner, M. Griebel, *J. Phys. Chem. B* **2002**, *106*, 3046.
[38] E. J. Wallace, M. S. P. Sansom, *Nano Lett.* **2007**, *7*, 1923.
[39] Q. Z. Xue, Q. B. Zheng, D. Xia, K. Y. Yan, X. L. Gao, Q. Li, *Appl. Surf. Sci.* **2009**, *255*, 3534.
[40] K. Liao, S. Li, *Appl. Phys. Lett.* **2001**, *79*, 4225.
[41] M. Wong, M. Paramsothy, X. J. Xu, Y. Ren, S. Li, K. Liao, *Polymer* **2003**, *44*, 7757.
[42] E. Munoz, A. B. Dalton, S. Collins, M. Kozlov, J. Razal, J. N. Coleman, B. G. Kim, V. H. Ebron, M. Selvidge, J. P. Ferraris, R. H. Baughman, *Adv. Eng. Mater.* **2004**, *6*, 801.
[43] T. Filleter, S. Yockel, M. Naraghi, J. T. Paci, O. C. Compton, M. L. Mayes, S. T. Nguyen, G. C. Schatz, H. D. Espinosa, *Nano Lett.* **2012**, *12*, 732.

[44] B. Chen, M. Gao, J. M. Zuo, S. Qu, B. Liu, Y. Huang, *Appl. Phys. Lett.* **2003**, *83*, 3570.
[45] K. M. Liew, C. H. Wong, M. J. Tan, *Appl. Phys. Lett.* **2005**, *87*, 041901.
[46] K. M. Liew, C. H. Wong, M. J. Tan, *Acta Mater.* **2006**, *54*, 225.
[47] W. Zhou, Y. Huang, B. Liu, K. C. Hwang, J. M. Zuo, M. J. Buehler, H. Gao, *Appl. Phys. Lett.* **2007**, *90*, 073107.
[48] C. Zhu, Z. Xie, K. Guo, *Diamond Relat. Mater.* **2004**, *13*, 180.
[49] M. J. Buehler, A. C. T. van Duin, W. A. Goddard, *Phys. Rev. Lett.* **2006**, *96*, 095505
[50] S. Cranford, H. Yao, C. Ortiz, M. J. Buehler, *J. Mech. Phys. Solids* **2010**, *58*, 409.
[51] S. Cranford, M. J. Buehler, *Int. J. Mater. Struct. Integr.* **2009**, *3*, 161.
[52] Y. Zhu, H. D. Espinosa, *Proc. Natl. Acad. Sci. USA* **2005**, *102*, 14503.
[53] C. A. Cooper, S. R. Cohen, A. H. Barber, H. D. Wagner, *Appl. Phys. Lett.* **2002**, *81*, 3873.
[54] S. J. Plimpton, *J. Comput. Phys.* **1995**, *117*, 1.
[55] C. A. Clifford, M. P. Seah, *Nanotechnology* **2005**, *16*, 1666.